J Comput Aided Mol Des (2010) 24:225–235
DOI 10.1007/s10822-010-9328-6

Conformational landscape of platinum(II)-tetraamine complexes: DFT and NBO studies

Austin B. Yongye · Marc A. Giulianotti · Adel Nefzi · Richard A. Houghten · Karina Martínez-Mayorga

Received: 28 January 2010 / Accepted: 9 March 2010 / Published online: 24 March 2010

Abstract The potential energy surfaces of chiral tetraamine Pt(II) coordination complexes were computed at the B3LYP/LANL2DZ level of theory by a systematic variation of two dihedral angles: C12–C15–C34–C37 (θ) and C24–C17–C31–C48 (ψ) employing a grid resolution of 30°. Potential energy surfaces calculated using density functional theory methods and Boltzmann-derived populations revealed strong preference for one diasteromer of each series studied. In addition, natural bond orbital analysis show that the minima are stabilized predominantly by a combination of electronic interactions between two phenyl groups, the phenyl groups and the Pt^{2+} ion, as well as with the amine groups. Additional experimental characterization of the diasteroisomers studied here is in progress and will permit further molecular modeling studies with the appropriate stereochemistry.

Keywords Conformational analysis · Platinum(II)-tetraamine complexes · Natural bond orbital · Potential energy surface

Introduction

Transition metal (TM) coordination complexes exhibit remarkable pharmacological properties that have led to their application as antiviral [1, 2], antimicrobial [3, 4] and antitumor [5, 6] agents. These biological properties have served as an impetus for the investigation of TM-ligand complexes as potential therapeutic compounds [7–10]. In these complexes, the metals may exert their influence by coordinating with atoms in a receptor, binding directly with biomolecules, or by inducing the formation of well-defined molecular architectures from which key ligand pharmacophores are presented to a receptor [6, 7, 11]. This structure-directing role is attractive because TMs can accommodate several frameworks that are not readily observed in typical organic compounds [7]. For instance, TMs have been utilized to generate three-dimensional globular topographies that display structural and functional group complementarities with the active sites of protein kinases [7]. In addition, their complexes have been employed as mimics of natural products [7, 12] or peptide turn inducers [7]. These examples indicate that the chemical space of biologically-relevant molecules, which has been heavily confined to organic compounds, may be expanded by the inclusion of TM-complexes.

There has been considerable interest in platinum-containing compounds ever since the seminal demonstration of the potency of the prototypical antitumor platinum-containing compound, *cis*-diamine-dichloro-platinum(II) or *cis*-platin [13, 14]. In spite of the benefits of *cis*-platin as a cancer cell DNA-cleaving agent, it displays undesirable side effects such as neurotoxicity and nephrotoxicity [15]. Moreover, there are reports about resistance to *cis*-platin [16] and its inactivity toward colorectal cancer [17]. Therefore, the development of less toxic but more broadly applicable metal-based biological and anticancer agents remains an area of active research.

For more than two decades the deconvolution of mixture-based combinatorial libraries has led to the identification of

Electronic supplementary material The online version of this article (doi:10.1007/s10822-010-9328-6) contains supplementary material, which is available to authorized users.

A. B. Yongye · M. A. Giulianotti · A. Nefzi · R. A. Houghten · K. Martínez-Mayorga (✉)
Torrey Pines Institute for Molecular Studies, 11350 SW Village Parkway, Port St. Lucie, FL 34987, USA
e-mail: kmartinez@tpims.org

bioactive compounds [18–20]. However, only few combinatorial libraries of metal-containing complexes have been explored so far for finding therapeutic agents [9, 12, 21, 22]. A combinatorial library generated from the D- and L-isomers of the Phe-Phe-Ala tripeptide has been recently reported [21]. By virtue of the presence of the chiral Cα atoms, this tripeptide inherently possesses three chiral centers. Upon reduction and complexation with the central Pt(II) ion two more chiral centers are produced at the nitrogen atoms of the secondary amines. One advantage of utilizing amino acids is the ease with which large combinatorial libraries can be generated by combining different amino acids and different stereochemistries [20]. Moreover, reduced polypeptides may be envisaged as polyamine scaffolds bearing protruding side chains exposed to a given target. Thus, combinatorial libraries of peptides and peptidomimetics are a very versatile source of compounds with controlled stereochemistry. While an RP-HPLC analysis of the mixtures indicated clear preferences for specific stereoisomers of the secondary amines, assigning these stereoisomers to specific peaks was challenging. Nonetheless, it is expected that their relative abundance would be governed by their thermodynamic stabilities. In the absence of a clear experimental resolution of the stereoisomers, quantum mechanical methods can be employed not only to provide information about conformational preferences of the Pt(II)-tetra-amine complexes, but also to help rationalize the origin of such preferences.

Towards the understanding of the conformational preferences and stabilizing interactions on Platinum-polyamine complexes, we employed quantum mechanical methods on a series of N′-[2-Amino-1-benzylethyl]-N″-[2-aminopropyl]-3-phenylpropane-1,2-diamineplatinum(II) diastereoisomers recently reported [21]. Despite the availability of ab initio [23] and X-ray crystallography data for other biologically active Pt(II)-amine complexes [24–29], to the best of our knowledge this is the first systematic characterization of the conformational landscape of metal-polyamine complexes of this type. Employing density functional theory methods we computed the potential energy surfaces of five diastereoisomers and determined their relative stabilities. Then, Natural Bond Orbital (NBO) analysis was employed to rationalize the origin of such conformational preferences. Optimization of synthetic methods along with a deeper understanding of stabilizing factors will aid the design of new metal-based compounds and chemical libraries of this class.

Results and discussion

Scheme 1 sketches (without defining stereochemistry) the chemical structure and the synthetic route of the Pt (II)-polyamine complexes studied in this work. The stereochemistry of the chiral centers bearing the R-groups are controlled by selecting amino acids with the appropriate chiralities as starting materials. The absolute configurations of each of the R-groups in the chiral tetraamines studied here are: *RRR, SSS, RSS*, *SRS* and *SSR*. Upon reduction of the amino acids followed by complexation with Pt(II) two additional stereogenic centers are generated at the secondary amine nitrogen atoms, Fig. 1. As a result, four diastereoisomers are produced, per chiral tetramine Pt(II) complex formed, with the following absolute configurations at the two secondary nitrogen atoms: *RR*, *RS*, *SR* and *SS*, for a total of 20 molecules: *RRR_RR, RRR_RS, RRR_SR, RRR_SS; SSS_RR, SSS_RS, SSS_SR, SSS_SS; RSS_RR, RSS_RS, RSS_SR, RSS_SS; SSR_RR, SSR_RS, SSR_SR, SSR_SS.* It should be noted that the *RRR* and *SSS* series are in effect mirror images containing the respective enantiomeric pairs (*RRR_RR/SSS_SS*, *RRR_RS/SSS_SR*, *RRR_SR/SSS_RS*, and *RRR_SS/SSS_RR*).

Potential energy surfaces and relative populations of the chiral tetraamine Pt(II) diasteroisomers

The potential energy surfaces (PES) of the four possible diasteromers of the *RRR* and *SSS* chiral tetramine Pt(II) complexes investigated in this work are illustrated in Fig. 2. The grid-spacing selected (30°) allowed for the identification of both low and high energy conformers, 2D projections are depicted at the top of the graphs. The PES for the *SRS*, *RSS* and *SSR* series are provided as contour maps in the supplementary material, Fig. S1.

From the PES presented in Fig. 2 it is possible to know which isomers are more stable (global minimum) as well as their conformational freedom (local minima). In some cases, like the isomer RRR_RS the PES shows that many conformations can be reach with changes in energy of ~4 kcal/mol. However, in other cases like in the RRR_RR isomer local minima are connected via less stable conformers ($\Delta E > 10$ kcal/mol). In the real world, the energy to reach different conformational states is overcome by interactions with the solvent or, in the case of biological systems, from the interaction with a biological target. A wide range of conformational penalties for bioactive conformations have been suggested; ranging from 3 [30] to more than 10 kcal/mol [31, 32]. From Fig. 2 it can be observed that in the RRR_SS and SSS_RR complexes the transition to different conformers requires small amount of energy, whereas for the RRR_RR and SSS_SS complexes high energy conformers populate the PES. It is expected that the PES with the consideration of explicit solvent will differ from those shown in Fig. 2 leading to different ratios among the diasteromers of each chiral tetramine Pt(II)

Scheme 1 **a** BF_3–THF, 65 °C, 4 days; **b** HF, anisole, 0 °C, 7 h; **c** K_2PtCl_4, DIPEA, DMF/H_2O (50/50), 60 °C, 48 h

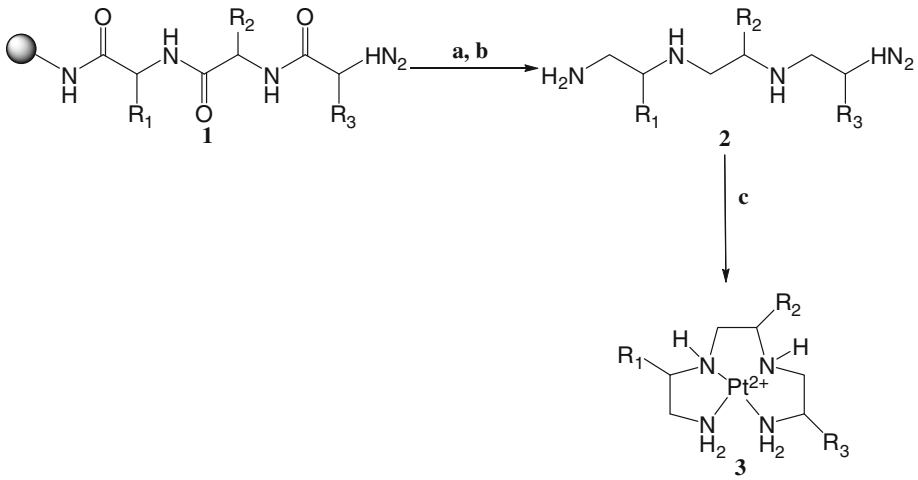

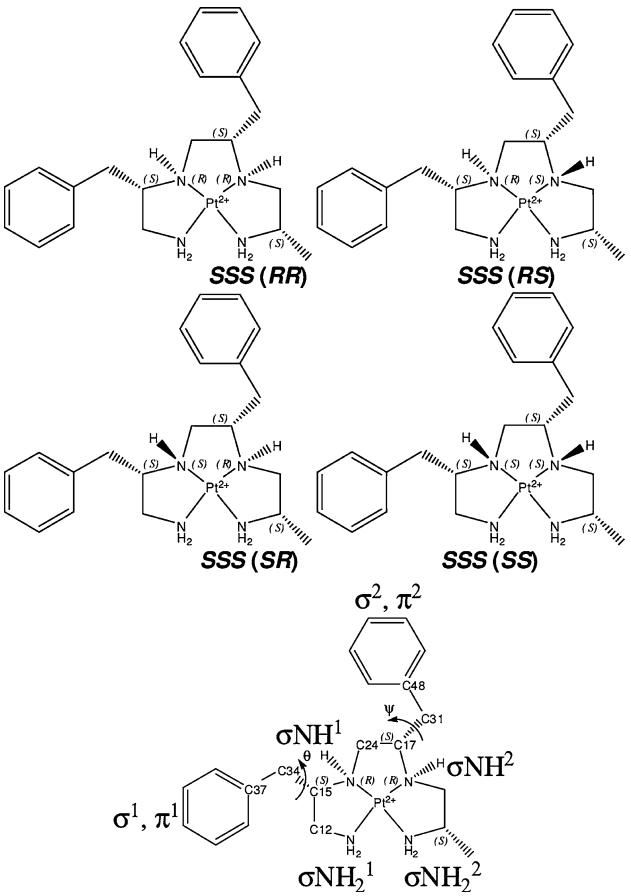

Fig. 1 The four possible diasteromers of the *SSS* tetraamine Pt(II) complex are the top and central structures. The atom names and numbers that define the (θ, ψ) angles are shown at the bottom σ and π denote potential sources of intra-molecular interactions

complex; however, the same dominant conformations are expected to remain (see below).

Although the grid size of 30° employed to generate the PES resulted in the identification of minimum and maximum stationary points, it was conceivable that a more refined grid would reveal the true global minimum of these isomers. Therefore, unrestrained QM optimizations were performed starting from the final coordinates of each restrain global minimum identified from the restrained conformational searches. The structure of each isomer at the corresponding global minimum is shown in Fig. 3. Differences in the energies and dihedral angles between the final structures of the restrained and unrestrained optimizations are presented in Table 1. In some cases, the differences in the (θ, ψ) values from both optimizations were significant, but in all cases they fell within the imposed grid points, with energy differences within 1.0 kcal/mol. The structural differences were directly correlated with the energy differences, exemplified in the *SRS_RS* and *SRS_SR* isomers. The ($\Delta\theta$, $\Delta\psi$) values for the *SRS_RS* isomer were (0°, 3°) and the ΔE value was −0.042 kcal/mol, while the ($\Delta\theta$, $\Delta\psi$) and ΔE values for the *SRS_SR* isomer were (10°, 15°) and −0.679 kcal/mol, respectively. The ($\Delta\theta$, $\Delta\psi$) values for the *RRR_SR*, *RSS_RS*, and *SRS_SR* were: (11°, 16°), (12°, 14°) and (10°, 15°), respectively, and the ΔE values were −0.668, −0.630, and −0.679 kcal/mol, respectively, suggesting that these minima were located in broad wells on the PES. In all the other cases, changes in the structure and in the energy were even smaller.

The Boltzmann population analyses of all the isomers studied utilizing the relative energies of the global minima determined from the restraint-free optimizations are summarized in Table 2 and depicted in Fig. 4. The relative energies (kcal/mol) in the RRR and SSS complexes were: RRR, SS (0) < RS (1.43) < SR (2.08) < RR (3.91); and SSS, RR (0) < RS (3.57) < SR (3.89) < SS (6.62). The corresponding Boltzmann populations (%) were: *RRR*, *SS* (72.24) > *RS* (17.29) > *SR* (9.02) > *RR* (1.45); and *SSS*, *RR* (95.24) > *RS* (2.68) ~ *SR* (1.95) > *SS* (0.13), respectively, Fig. 4. The relative populations indicated that within each series of chiral tetramine Pt(II) complexes specific diasteroisomers were strongly preferred, although

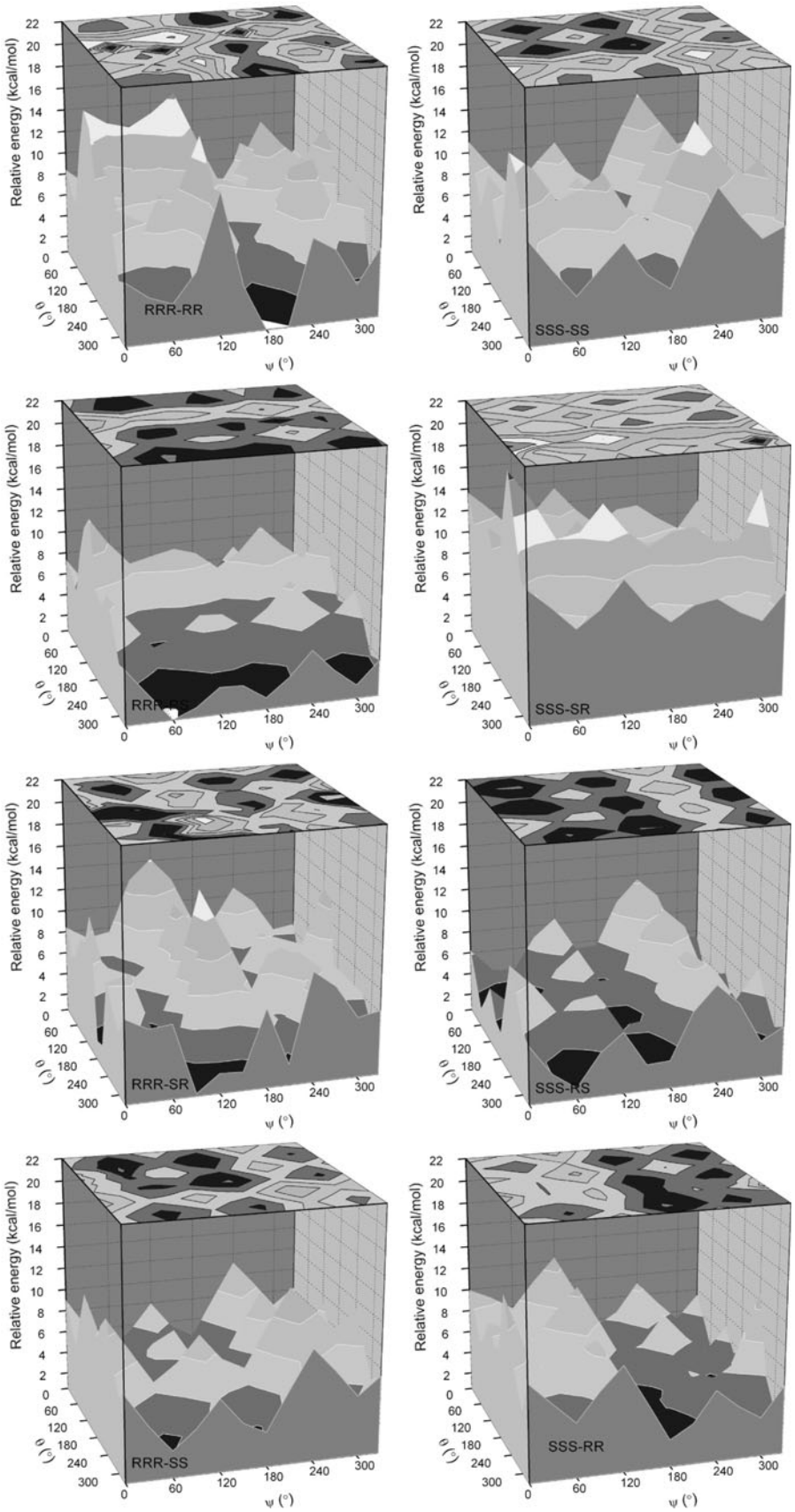

Fig. 2 B3LYP/LANL2DZ conformational energy landscapes for the each of the four diastereomers of the *RRR* (*left*) and *SSS* (*right*) series. The 2D projections of the energy landscapes are shown on the *top* of each plot

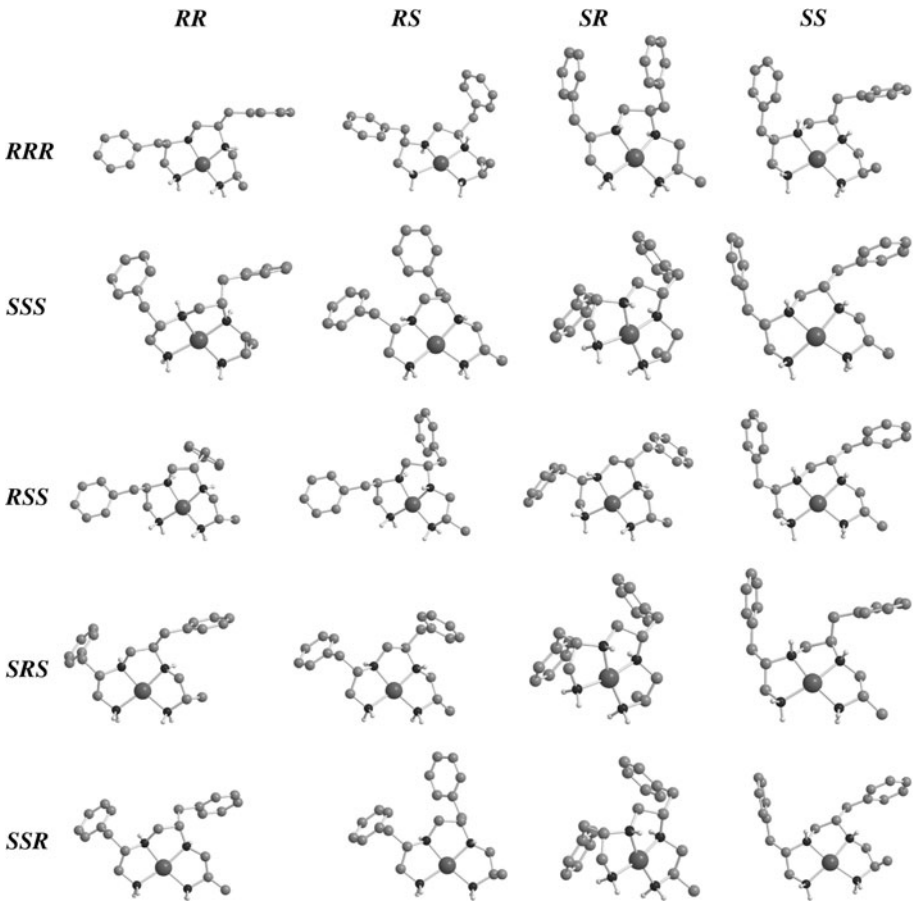

Fig. 3 The lowest energy structures identified from the potential energy surfaces of each diasteromer of the *RRR*, *SSS*, *RSS*, *SRS*, and *SSR* tetraamine Pt(II) complexes

there were secondary populations of the other diasteroisomers. For instance, the *SS* (72.24%) and *RR* (95.24%) diasteroisomers were predominant within the *RRR* and *SSS* series, respectively, while the SR and RS isomers were also populated, albeit in smaller proportions. It is interesting to note the mirror-image relationship between the relative abundance of these two series. In the *RRR* series, the *RR* and *SS* diasteroisomers were the most and least populated, respectively, while in the *SSS* series the exact opposite was observed. However, the relationship between the *RS* and *SR* isomers was not definitive. This inconsistency may be ascribed to the 1 kcal/mol difference in the relative energies of the *RS* and *SR* isomers, rendering the prediction of their relative stabilities quite challenging for most theoretical methods [33]. In order to refine the calculations a more comprehensive conformational search could be performed for instance by the modification of the dihedral angle that affects the rotation of the phenyl groups (CH_2-C_{ipso}); even though that dihedral angle was not restrain during the optimization, it is possible that it reached a local minimum. Nevertheless, in both cases a predominance of one isomer was observed, while the others were present in smaller quantities. The predominance of a single diasteroisomer was also observed for the *SRS*, *SSR* and *RSS* complexes. The relative energies of the isomers, *SRS* and *SSR*, were: *SRS*, *RS* (0) < *RR* (4.58) ~ *SS* (4.64) < *SR* (9.29); and *SSR*, *RR* (0) < *SR* (3.65) < *RS* (6.71) < *SS* (9.54), resulting in the following Boltzmann populations (%): *SRS*, *RS* (98.04) > *RR* (1.01) ~ *SS* (0.95) > *SR* (0.01); and *SSR*, *RR* (97.34) > *SR* (2.53) > *RS* (0.11) > *SS* (0.01). These populations also pointed to the prevalence of one diasteroisomer in each series. For the *RSS* diasteromers, the B3LYP/LANL2DZ determined relative energies were: *RSS*, *SR* (0) < *SS* (1.49) ~ *RR* (1.77) < *RS* (2.90), with corresponding Boltzmann populations (%) of *RSS*, *SR* (68.93) > *SS* (15.54) > *RR* (11.74) > *RS* (3.79), once more depicting a high proportion for one diasteroisomer. As a rough comparison the RP-HPLC spectra for all the series also show one preferred diasteroisomer on each series. RP-HPLC spectra for the SRS, SSR, and RSS complexes are presented as supplementary material, Fig. S2; for the RRR and SSS series they have been previously published [21]. Albeit the full experimental characterization of each diasteromer and further calculations will be required, the HPLC shows a clear predominance of one diasteromer of each series.

Table 1 Energies obtained from the optimization of the chiral tetraamine Pt(II) complexes using Gaussian 03 at B3LYP/LANL2DZ level of theory for the RRR, SSS, RSS, SRS and SSR series

	Restricted			Full optimization					
	E (Hartrees)	θ (°)[a]	ψ (°)[b]	E (Hartrees)	θ (°)[a]	ψ (°)[b]	$\Delta\theta$	$\Delta\psi$	ΔE (kcal/mol)[c]
RRR_RR	−1157.0934614	300	180	−1157.0940242	311	184	11	4	−0.353
***RRR**_RS*	−1157.09736882	300	60	−1157.09774930	314	63	14	3	−0.239
RRR_SR	−1157.09633419	180	300	−1157.09739840	191	316	11	16	−0.668
RRR_SS	−1157.09964513	180	180	−1157.10025100	174	172	6	8	−0.380
SSS_RR	−1157.1029649	300	180	−1157.1033911	296	188	4	8	−0.267
***SSS**_RS*	− 1157.0974459	300	60	−1157.0976988	306	61	6	1	−0.159
SSS_SR	−1157.0965351	300	300	−1157.0971854	309	298	9	2	−0.408
SSS_SS	−1157.0924818	180	180	−1157.092838	176	173	4	7	−0.224
RSS_RR	−1157.0962740	300	300	−1157.0968958	311	295	11	5	−0.390
***RSS**_RS*	−1157.0940972	300	30	−1157.0951015	312	44	12	14	−0.630
RSS_SR	−1157.0994490	60	300	−1157.0997186	65	297	5	3	−0.169
RSS_SS	−1157.0967983	180	180	−1157.0973362	173	175	7	5	−0.338
SRS_RR	−1157.0982023	300	180	−1157.0985953	295	187	5	7	−0.247
***SRS**_RS*	−1157.1054976	300	60	−1157.1055641	300	63	0	3	−0.042
SRS_SR	−1157.0907107	300	330	−1157.0917935	310	315	10	15	−0.679
SRS_SS	−1157.0981038	180	180	−1157.0984532	177	172	3	8	−0.219
SSR_RR	−1157.105540	300	180	−1157.105937	295	188	5	8	−0.250
***SSR**_RS*	−1157.094905	300	60	−1157.095240	306	61	6	1	−0.210
SSR_SR	−1157.099351	300	300	−1157.100119	311	295	11	5	−0.482
SSR_SS	−1157.090381	180	180	−1157.090727	176	173	4	7	−0.217

a Atom number: C12–C15–C34–C37; b Atom number: C24–C17–C31–C48; c Full optimization—Restricted optimization

Stabilizing factors in the chiral tetraamine Pt(II) complexes

It is expected that the stability of each conformer will be affected by steric factors that are readily discernable. Beyond steric considerations electronic delocalization may also influence the stabilities of the chiral tetraamine Pt(II) complexes. To identify the degree of stabilization afforded by interactions due to electronic delocalization the NBO program [34] was employed; intramolecular interactions were evaluated between key functional groups in minimum stationary point structures whose relative energies were within 2.0 kcal/mol of their respective global minimum. The deletions involved interactions between the following groups: aromatic phenyl–phenyl interactions (π–π sandwich and π–σ T-shaped); phenyl–Pt(II) (π–Pt(II)); and phenyl-amine interactions (π–σ). Selected minima exhibiting these interactions are portrayed in Fig. 5, and the energetic contributions of these interactions in the global minimum of each diasteroisomer are presented in Table 3. A complete list of interactions in conformers within 2.0 kcal/mol of their respective global minima is given in Tables S1–S5 of the supplementary section. Various combinations of these interactions were observed in the local and global minimum structures identified. The superscripts denote the phenyl group of a given R_i substituent, Fig. 1. The origins of these interactions could be explained by examining the structures of some conformers. For example the π^2–Pt^{2+} interaction in the (300°, 300°) global minimum point of the *SSS_SR* isomer is apparent (Fig. 5). However, less intuitive interactions were observed between phenyl groups and NH bond vectors. Nonetheless, the energy increase observed when these interactions were suppressed pointed to their relevance in stabilizing the respective conformers. The significance of the effects of electronic stabilizations were apparent by their occurrence in three-quarters (15 out of 20) of the global minima identified on the PES of these isomers. Conformers that did not exhibit discernable intramolecular electronic interactions (denoted "no sterics") consistently produced the lowest deletion energies when these interactions were suppressed. The conformers of these global minima included: *RRR_RR*, *SSS_SS*, *RSS_RS* and *SSR_SS* with deletion energies of 2.3, 2.0, 1.3 and 2.1 kcal/mol, respectively, Table 3. On the other hand, conformers wherein either one or both phenyl groups were prevented from interacting with the central Pt^{2+} ion always displayed high deletion energies, for example the *SSS_SR*, *SRS_SR* and *SSR_SR* conformers with deletion energies of 16.7, 17.5 and 17.2 kcal/mol, respectively.

Table 2 Minimum energy obtained for the full optimization of the isomers RR, RS, SR, and SS using Gaussian 03 at B3LYP/LANL2DZ level of theory for the RRR, SSS, RSS, SRS and SSR series

	E (Hartrees)	ΔE (kcal/mol)[a]	Population (%)	θ^b	ψ^c
RRR_RR	−1157.0940242	3.91	1.45	311	184
***RRR**_RS*	−1157.09774930	1.43	17.29	314	63
RRR_SR	−1157.09739840	2.08	9.02	191	316
RRR_SS	−1157.10025100	0	72.24	174	172
SSS_RR	−1157.1033911	0	95.24	296	188
***SSS**_RS*	−1157.0976988	3.57	2.68	306	61
SSS_SR	−1157.0971854	3.89	1.95	309	298
SSS_SS	−1157.092838	6.62	0.13	176	173
RSS_RR	−1157.0968958	1.77	11.74	311	295
***RSS**_RS*	−1157.0951015	2.9	3.79	312	44
RSS_SR	−1157.0997186	0	68.93	65	297
RSS_SS	−1157.0973362	1.49	15.54	173	175
SRS_RR	−1157.0985953	4.58	1.01	295	187
***SRS**_RS*	−1157.1055641	0	98.04	300	63
SRS_SR	−1157.0917935	9.29	0.01	310	315
SRS_SS	−1157.0984532	4.64	0.95	177	172
SSR_RR	−1157.105937	0	97.34	295	188
***SSR**_RS*	−1157.095240	6.71	0.11	306	61
SSR_SR	−1157.100119	3.65	2.53	311	295
SSR_SS	−1157.090727	9.54	0.01	176	173

a Relative energies; b Atom number: C12–C15–C34–C37; c Atom number: C24–C17–C31–C48

Overall, the strengths of the electronic stabilization could be ranked as follows: aromatic π-π < aromatic π–σ < aromatic π–σ NH/NH_2 < π–Pt^{2+}. In one conformer, *RSS_RS*: (60°, 300°), both phenyl groups enclosed the Pt^{2+} ion above and below the plane formed by the four coordinating amine groups. Deleting all intramolecular interactions in this conformer resulted in the highest deletion energy with a value of 27.8 kcal/mol. It was also observed that the electronic contributions in some local minima were stronger relative to their global minima, indicating that there is a collective contribution from both electronic and steric factors in determining the stabilities of these tetraamine Pt(II) complexes.

Geometry of the coordination complex

Finally we sought to elucidate the coordination geometry of the chiral tetraamine Pt(II) complexes. Selected distances and angles of each global minimum minimized without restraints are summarized in Table 4. Atom names are shown in Fig. 6. The four amine nitrogen atoms were almost equidistant from the Pt(II) ion in all the stereoisomers. However, closer examination indicated that there were two sets of Pt(II)–N distances that could be distinguished: Pt(II) to the secondary amine nitrogen atoms (N2, N4), and Pt(II) to the primary amine nitrogen atoms (N3, N5), with the former being slightly shorter. For example in the *RRR_RS* isomer the Pt–N2 and Pt–N4 distances were 2.055 and 2.059 Å, respectively, both shorter than the Pt–N3 and Pt–N5 distances of 2.118 and 2.116 Å, respectively, Table 4. Furthermore, the computed averages for all the Pt(II)–N distances in all the isomers: Pt–N2 (2.057 ± 0.00 Å) Pt–N4 (2.057 ± 0.01 Å), Pt–N3 (2.111 ± 0.00 Å) and Pt–N5 (2.114 ± 0.00 Å) confirmed the presence of two different sets of distances. A plausible explanation of these differences is that the primary amine groups were less constrained during optimizations, giving rise to a significant degree of movement away from the central Pt(II) ion. The experimental structures of some related Pt(II)-complexes with biological relevance have been elucidated via both theoretical methods using effective core potential (ECP) and a variety of basis sets [23], as well as with experimental X-ray methods [24–29]. The principal difference between the structures studied previously and the tetraamine investigated here is that the tetraamine is a single multidentate ligand that provides all the chelating moieties, while the previously reported structures comprised multiple ligands.

This difference also suggests that the clear dichotomy in the values of the distances observed in the tetraamine studied in this work may not be observed in the previous complexes. Among the experimental structures reported previously there were notable differences in the Pt(II)–N bond lengths, indicating that the environment of the central atom and possibly crystal packing may influence these geometrical values. For instance, the platinum–nitrogen distances in the experimental studies [24–29] ranged from 1.998 [27] to 2.121 Å [24]. Theoretical ab initio distances computed at the HF/LANL2DZ level of theory were 2.100 and 2.148 Å [23]. Nonetheless, these theoretical and experimental distances were in range with the averages determined in this work: 2.057 ± 0.00, 2.057 ± 0.01, 2.111 ± 0.00 and 2.114 ± 0.00 Å.

The bond angles subtended by the nitrogen atoms at the Pt(II) atom also showed some interesting trends. The average angle between the primary amines, N3–Pt–N5, was 106.26 ± 1.3°, while the angle between the secondary amines, N2–Pt–N4, was remarkably smaller, 86.02 ± 0.6°. Furthermore, the averages of the angles formed between the primary and secondary amines were much smaller, 83.77 ± 0.9° and 83.91 ± 1.0° for the N2–Pt–N3 and N4–Pt–N5 atoms, respectively.

These trends may be ascribed to the compression of the N2–Pt–N3 and N4–Pt–N5 angles due to the expansion of the N3–Pt–N5 angle between the primary amines during optimization. It should be noted that the average value obtained here for the N3–Pt–N5 bond angle

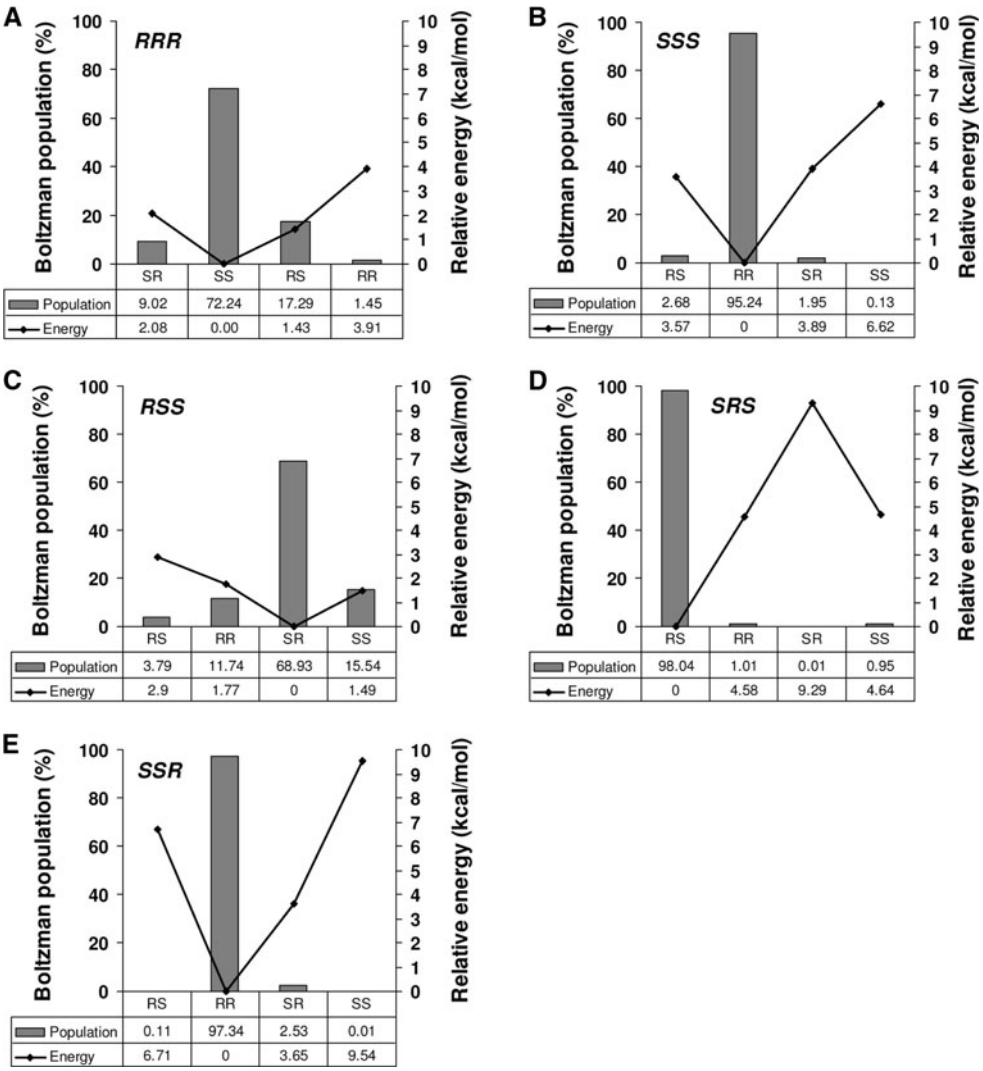

Fig. 4 The B3LYP/LANL2DZ relative energies and the corresponding Boltzmann population distributions

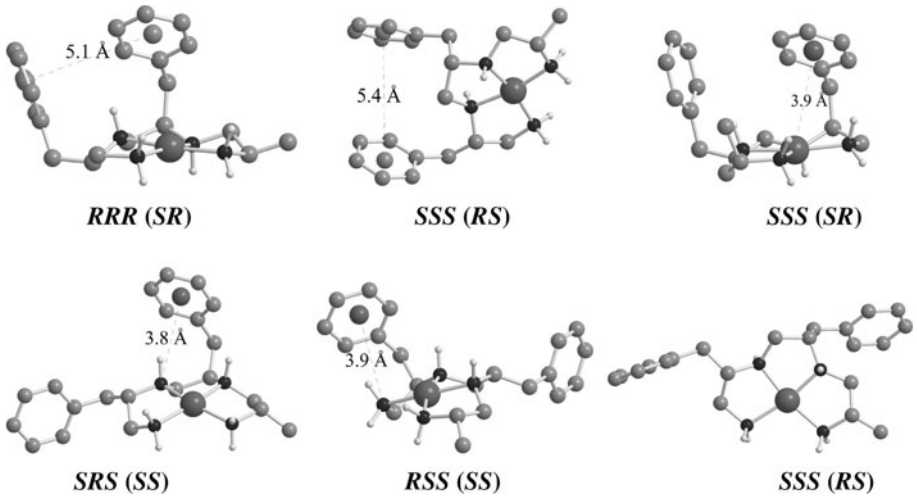

Fig. 5 Intramolecular interactions in selected conformations of the Pt^{2+}-polyamine complexes. ***RRR_SR***: T-shaped π^2–σ^1; ***SSS_RS***: Sandwich π^1–π^2; ***SSS_SR***: π^1–Pt^{2+}; ***SRS_SS***: π^2–σNH^1; ***RSS_SS***: π^1–σ NH_2^1; ***SSS_RS***: No sterics

(106.26 ± 1.3°) differed from the experimental range, 82.7° [29] to 92.5° [28], reported in the literature [24–29]. This discrepancy may be due to structural differences in the types of ligands, crystal packing or the environments in which these crystals were obtained. To completely define the coordination geometry, the angles between the *anti*

Table 3 Intramolecular interactions that drive the stabilities of the global minima of the chiral tetraamine Pt(II) complexes

	(θ, ψ)	Interaction (distances Å)[a]	Deletion energy[b]
RRR	*RR* (300, 180)	No sterics	2.3
	RS (300, 60)	"	4.0
	SR (180, 300)	π^1–π^2 (5.7)	2.1
	SS (180, 180)	π^1–σ NH^1 (4.0), π^2–σ NH^2 (3.9)	7.2
RSS	*RR* (300, 300)	π^2–NH^1 (3.9)	8.5
	RS (300, 30)	No sterics	1.3
	SR (60, 300)	π^1–σ NH_2^1 (3.9), π^1–σ NH^1 (4.0), π^2–σ NH^2 (4.1)	9.4
	SS (180, 180)	π^1–σ NH^1 (4.0)	5.3
SSR	*RR* (300, 180)	π^1–σ NH^1 (4.0)	6.7
	RS (300, 60)	π^2–σ^1 (5.7), π^1–σ NH^1 (4.0)	6.1
	SR (300, 300)	π^2–Pt^{2+} (3.8), π^1–π^2 (5.6)	17.2
	SS (180, 180)	No sterics	2.1
SSS	*RR* (300, 180)	π^1–σ NH^1 (4.2), π^2–σ NH^2 (4.1)	6.8
	RS (300, 60)	π^2–σ^1 (6.0), π^1–σ NH^1 (4.1)	5.9
	SR (300, 300)	π^2–Pt^{2+} (3.9), π^1–σ^2 (5.7)	16.7
	SS (180, 180)	No sterics	2.0
SRS	*RR* (300, 180)	π^1–σ NH^1 (3.9), π^2–σ NH^2 (4.1)	4.6
	RS (300, 60)	π^1–σ NH^1 (4.2), π^2–σ NH^2 (4.1)	5.9
	SR (300, 330)	π^1–Pt^{2+} (4.1), π^2–σ NH^1 (4.1)	17.5
	SS (180, 180)	π^1–σ NH^1 (4.1), π^2–σ NH^2 (4.0)	11.7

a Superscripts signify the sequential occurrence of the interacting groups, e.g. π^2–σ NH^1 represents a π-interaction between the second phenyl group and a σ-interaction with the first NH group. Distances between the groups are given in parentheses. The geometric centers of the phenyl groups were employed to determine interactions distances. b Energetic effect of deleting certain interaction, kcal/mol

Table 4 Selected distances (Å) and angles (°) of the global minimum of each chiral tetraamine Pt(II) complex computed using Gaussian 03 at B3LYP/LANL2DZ level of theory for the *RRR*, *SSS*, *RSS*, *SRS* and *SSR* series

	Pt–N2	Pt–N3	Pt–N4	Pt–N5	N3–Pt–N5	N2–Pt–N3	N4–Pt–N5	N2–Pt–N4	N3–Pt–N4	N2–Pt–N5
RRR_RR	2.059	2.109	2.064	2.111	105.49	84.29	84.48	86.34	170.45	166.67
RRR_*RS*	2.055	2.118	2.059	2.116	107.30	83.27	83.79	86.23	168.24	167.43
RRR_SR	2.063	2.118	2.055	2.115	106.74	83.85	83.31	86.58	168.26	168.77
RRR_SS	2.058	2.110	2.056	2.112	105.48	83.30	84.43	85.17	167.20	167.47
SSS_RR	2.053	2.111	2.051	2.117	105.05	84.71	84.10	85.66	169.96	167.32
SSS_*RS*	2.057	2.111	2.052	2.117	106.83	83.85	83.28	86.66	167.37	168.69
SSS_SR	2.050	2.112	2.053	2.114	107.11	83.31	83.88	86.35	168.20	167.42
SSS_SS	2.064	2.107	2.067	2.106	104.54	84.30	84.39	85.66	167.13	168.04
RSS_RR	2.054	2.110	2.055	2.117	106.05	84.76	84.35	84.84	169.59	167.54
RSS_*RS*	2.059	2.116	2.061	2.116	107.67	83.36	83.46	86.08	167.66	167.90
RSS_SR	2.051	2.108	2.053	2.114	109.18	80.69	83.80	86.95	166.42	167.94
RSS_SS	2.058	2.105	2.068	2.109	105.42	83.54	84.08	85.89	167.48	167.45
SRS_RR	2.054	2.110	2.064	2.115	104.66	84.50	83.98	86.24	170.10	167.37
SRS_*RS*	2.054	2.114	2.050	2.113	107.13	83.73	83.37	86.53	167.84	167.65
SRS_SR	2.052	2.109	2.060	2.118	107.58	83.25	83.57	86.13	167.77	168.08
SRS_SS	2.065	2.110	2.055	2.107	105.34	84.43	84.46	84.77	166.96	167.44
SSR_RR	2.054	2.110	2.052	2.113	105.25	84.70	83.89	85.68	169.94	167.32
SSR_*RS*	2.056	2.112	2.052	2.121	106.77	83.83	83.42	86.62	167.50	168.65
SSR_SR	2.050	2.110	2.053	2.110	107.26	83.36	83.64	86.36	168.21	167.62
SSR_SS	2.064	2.108	2.068	2.110	104.34	84.27	84.55	85.62	166.82	167.97

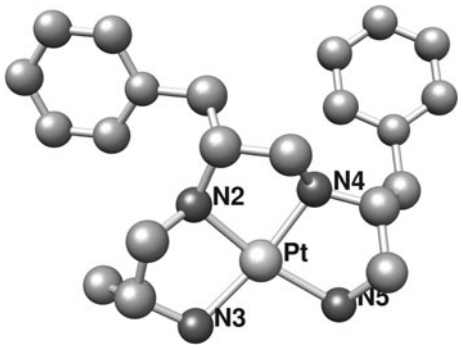

Fig. 6 Representation of the atom names employed to define bond lengths and angles around the central Pt(II) atom

N3–Pt–N4 and N2–Pt–N5 atoms were determined. The values were 168.16 ± 1.2° and 167.74 ± 0.5° for the N3–Pt–N4 and N2–Pt–N5 bond angles, respectively, indicating that the coordination geometry deviated from the ideal square-planar geometry, as also observed in the experimental structures. Taken together the angles between the pairs of adjacent nitrogen atoms, and between the pairs of *anti* nitrogen atoms indicated that the chelating amine groups adopted a distorted square-planar coordination geometry around the Pt(II) ion.

Conclusions

Conformational preferences of a series of chiral tetraamine Pt(II) complexes were performed using DFT methods. A Boltzmann population analysis showed that within each series of chiral tetraamine Pt(II) complexes, there are strong preferences for particular diasteroisomers, comparable to experimental preferences from RP-HPLC. NBO analysis showed that the stabilizing electronic delocalizations in increased order were π–Pt(II) > aromatic π–σ NH/NH2 > aromatic π–σ > aromatic π–π. The significance of the effects of electronic stabilizations was apparent by their occurrence in three-quarters of the global minima identified on the PES of these isomers. Conformers that did not exhibit discernable intramolecular electronic interactions consistently produced the lowest deletion energies when these interactions were suppressed. Thus, the electronic and steric factors that collectively contributed in the stabilization of these tetraamine Pt(II) complexes were evaluated. In addition, the geometrical analysis showed that the chelating amine groups adopted a distorted square-planar coordination geometry around the Pt(II) ion. Confrontation of the results obtained here with the experimental characterization, as well as application of this type of compounds as biological inhibitors to different targets is in progress.

Computational methods

The conformations of the stereoisomers were optimized utilizing the hybrid functional B3LYP with the LANL2DZ basis set, that implements the Dunning/Huzinaga full double zeta [35] basis set for H, C, N, and O atoms, and the Los Alamos ECP plus DZ [36–38] for platinum as suggested in previous studies involving organo-platinum complexes [23]. All calculations were carried out with the Gaussian 03 program (G03) [39] at the High Performance Computing Cluster of the Florida State University, Tallahassee, Florida. Visualization, input file preparation and analysis were performed employing the GaussView version 4.1 [40] software package. Energy surfaces were produced employing OriginLab v8.0. The conformational landscape of the four possible diasteroisomers of the *SSS*, and *RRR*, *RSS*, *SRS* and *SSR* series were produced by a systematic variation of the (θ, ψ) dihedral angles, Fig. 1, with a grid space of 30°. The *SSS* notation denotes the stereochemistry of the first, second and third Cα atoms in the reduced compound. The notation *SSS_SS* signifies that the chiralities of the first and second secondary amine nitrogen atoms are *S* and *S*, respectively. The 30° grid spacing resulted in 144 conformations per diasteromer, for a total of 2,880 conformers. The Gaussian 03 [39] default convergence criteria for energy minimization were employed. During energy minimization the Cartesian coordinates of the atoms defining θ (C12–C15–C34–C37) and ψ (C24–C17–C31–C48) were restrained at their respective grid points, while the rest of the molecule was allowed to relax. The global energy minimum of each complex was determined from the potential energy surface, minimized further without restraints, and the relative energies employed to predict its Boltzmann population, according Eq. 1:

$$P_i = \frac{\exp\left(-\frac{\varepsilon i}{RT}\right)}{\sum_{i=1}^{n} \exp\left(-\frac{\varepsilon i}{RT}\right)} \quad (1)$$

where *Pi* and ε_i are the Boltzmann population and relative energy, respectively, of the *i*th isomer; R = universal gas constant; T = room temperature. The energetic factors that contributed to the stabilities of these conformers were determined from natural bond orbital (NBO) analyses [34] performed on selected representative minima.

Acknowledgments This work was supported by the State of Florida, Executive Officer of the Governor's Office of Tourism, Trade and Economic Development, and by the National Science Foundation (CHE0455072 to R.A.H.). The authors thank the Florida State University High Performance Computing Facility for supercomputing time and Dr. Carmen Ortega-Alfaro for insightful discussions.

References

1. Sun RW-Y, Ma D-L, Wong EL-M, Che C-M (2007) Dalton Trans 43:4884–4892
2. Inouye Y, Kanamori T, Sugiyama M, Yoshida T, Koike T, Shionoya M, Enomoto K, Suehiro K, Kimura E (1995) Antivir Chem Chemother 6:337–344
3. Singh RV, Joshi SC, Kulshrestha S, Nagpal P, Bansal A (2001) Metal Based Drugs 8:149–158
4. Ming L-J, Epperson JD (2002) J Inorg Biochem 91:46–58
5. Hollis LS, Amundsen AR, Stern EW (1989) J Med Chem 32:128–136
6. Zheng H, Hu W, Yu D, Shen D-Y, Fu S, Kavanagh JJ, Wei I-C, Yang DJ (2008) Pharm Res 25:2272–2282
7. Meggers E (2007) Curr Opin Chem Biol 11:287–292
8. Orvig C, Abrams MJ (1999) Chem Rev 99:2201–2203
9. Bregman H, Carroll PJ, Meggers E (2006) J Am Chem Soc 128:877–884
10. Budzisz E, Malecka M, Lorenz I-P, Mayer P, Kwiecien RA, Paneth P, Krajewska U, Rozalski M (2006) Inorg Chem 45: 9688–9695
11. Lovejoy KS, Todd RC, Zhang S, McCormick MS, D'Aquino JA, Reardon JT, Sancar A, Giacomini KM, Lippard SJ (2008) Proc Natl Acad Sci USA 105:8902–8907
12. Williams DS, Carroll PJ, Meggers E (2007) Inorg Chem 46: 2944–2946
13. Rosenberg B, Van Camp L, Krigas L (1965) Nature 205:698–699
14. Rosenberg B (1985) Cancer 55:2303–2316
15. Ludwig T, Riethmuller C, Gekle M, Schwerdt G, Oberleithner H (2004) Kidney Int 66:196–202
16. Weiss RB, Christian MC (1993) Drugs 46:360–377
17. Zhang S, Lovejoy KS, Shima JE, Lagpacan LL, Shu Y, Lapuk A, Chen Y, Komori T, Gray JW, Chen X, Lippard SJ, Giacomini KM (2006) Cancer Res 66:8847–8857
18. Dooley CT, Chung NN, Wilkes BC, Schiller PW, Bidlack JM, Pasternak GW, Houghten RA (1994) Science 266:2019–2022
19. Houghten RA, Pinilla C, Appel JR, Blondelle sE, Dooley CT, Eichler J, Nefzi A, Ostresh JM (1999) J Med Chem 42:3743–3778
20. Pinilla C, Appel JR, Borras E, Houghten RA (2003) Nat Med 9:118–122
21. Nefzi A, Hoesl CE, Pinilla C, Kauffman GB, Maggiora GM, Pasquale E, Houghten RA (2006) J Comb Chem 8:780–783
22. Meggers E (2009) Chem Commun 1001–1010
23. Mora MA, Raya A, Mora-Ramirez MA (2002) Int J Quantum Chem 90:882–887
24. Hasinoff BB, Wu X, Yang Y (2004) J Inorg Biochem 98:616–624
25. Davies HO, Brown DA, Yanovsky AI, Nolan KB (1998) Inorg Chim Acta 268:313–316
26. Messori L, Shaw J, Camalli M, Mura P, Marcon G (2003) Inorg Chem 42:6166–6168
27. Granifo J, Vargas ME, Rocha H, Garland MT, Baggio R (2001) Inorg Chim Acta 321:209–214
28. Rotondo A (2006) Acta Crystallogr Sect C: Cryst Struct Commun 62:m19–m21
29. Hollis LS, Amundsen AR, Stern EW (1985) J Am Chem Soc 107:274–276
30. Liljefors T, Pettersson I (2002) In: Krogsgaard-Larsen P, Liljefors T, Madsen U (eds) Textbook of drug design and discovery. Taylor & Francis, London, pp 86–116
31. Perola E, Charifson PS (2004) J Med Chem 47:2499–2510
32. Butler KT, Luque FJ, Barril X (2009) J Comput Chem 30: 601–610
33. Yongye AB, Foley BL, Woods RJ (2008) J Phys Chem A 112: 2634–2639
34. Glendening ED, Badenhoop JK, Reed AE, Carpenter JE, Bohmann JA, Morales CM, Weinhold F (2001) Theoretical Chemistry Institute, University of Wisconsin, Madison: NBO 5.0
35. Dunning TH Jr, Hay PJ (1976) In: Schaefer HF III (ed) Modern theoretical chemistry. Plenum, New York, p 1
36. Hay PJ, Wadt WR (1985) J Chem Phys 82:270–283
37. Hay PJ, Wadt WR (1985) J Chem Phys 82:299–310
38. Wadt WR, Hay PJ (1985) J Chem Phys 82:284–298
39. Frisch MJ, Trucks GW, Schlegel HB, Scuseria GE, Robb MA, Cheeseman JR, Montgomery Jr. JA, Vreven T, Kudin KN, Burant JC, Millam JM, Iyengar SS, Tomasi J, Barone V, Mennucci B, Cossi M, Scalmani G, Rega N, Petersson GA, Nakatsuji H, Hada M, Ehara M, Toyota K, Fukuda R, Hasegawa J, Ishida M, Nakajima T, Honda J, Kitao O, Nakai H, Klene M, Li X, Knox JE, Hratchian HP, Cross JB, Adamo C, Jaramillo J, Gomperts R, Stratmann RE, Yazyev O, Austin AJ, Cammi R, Pomelli C, Ochterski JW, Ayala PY, Morokuma K, Voth GA, Salvador P, Dannenberg JJ, Zakrzewski VG, Dapprich S, Daniels AD, Strain MC, Farkas O, Malick DK, Rabuck AD, Raghavachari K, Foresman JB, Ortiz JV, Cui A, Baboul AG, Clifford S, Cioslowshi J, Stefanov BB, Liu G, Liashenko A, Piskorz P, Komaromi I, Martin RL, Fox DJ, Keith T, Al-Laham MA, Peng CY, Nanayakkara A, Challacombe M, Gill PMW, Johnson B, Chen W, Wong MW, Gonzalez C, Pople JA (2004)
40. Dennington II R, Keith T, Millam J (2007) Semichem Inc., Shawnee Mission, KS